JOURNAL OF GEOPHYSICAL RESEARCH, VOL. 103, NO. D20, PAGES 26,051–26,060, OCTOBER 27, 1998

Effect of aerosols on solar UV irradiances during the Photochemical Activity and Solar Ultraviolet Radiation campaign

A. Kylling,[1,2] A. F. Bais,[3] M. Blumthaler,[4] J. Schreder,[4] C. S. Zerefos,[3] and E. Kosmidis[3]

Abstract. Surface UV irradiances were measured at two different sites in Greece during June 1996 under noncloudy conditions. The measured UV irradiances are simulated by a radiative transfer model using measured ozone density and aerosol optical depth profiles. The absolute difference between model and measurements ranges between −5% and +5% with little dependence on wavelength. The temporal and solar zenith angle dependence in the difference between model and measurement suggests that part of this difference may be explained by assumptions made about the aerosol single–scattering albedo and phase function. Simulated spectra including aerosols are compared with calculated spectra excluding aerosols. It is found that for otherwise similar atmospheric conditions the UVB irradiance is reduced with respect to aerosol free conditions by 5% to 35% depending on the aerosol optical depth and single–scattering albedo. For the campaign period, changes in the aerosol loading gave larger variations in the surface UV irradiances than the changes seen in the ozone column.

1. Introduction

The relationship between ozone and surface UV irradiance is well established. While by far the largest changes in the surface UV irradiance are due to the predictable changes in the solar zenith angle, less is known about the effects of clouds and aerosols. In this paper the effect of aerosols on surface UV irradiances will be investigated.

A number of studies have explored the effect of stratospheric aerosols on the UV radiation field. Comparatively fewer have examined the effect of tropospheric aerosols on the surface UV irradiance. *Liu et al.* [1991] used satellite measurements of the ozone column and ground–based measurements of the visibility together with model calculations to investigate the impact of anthropogenic aerosols on biologically active ultraviolet radiation in industrialized countries. They found that UVB (280–315 nm) radiation had decreased by 5–18% in nonurban areas since the industrial revolution as a result of aerosol formed from emissions of SO_2. *Mayer et al.* [1997] reported a detailed measurement/model comparison covering a wide variety of ozone and aerosol conditions and a long time period. Using standard ozone and aerosol profiles scaled to measured column values, they found systematic differences between −11% and +2% for the wavelength range 295 to 400 nm when comparing more than 1200 measured spectra covering a 2 year period, with model simulations. Hence detailed model calculations may reproduce UV measurements within the error bounds associated with these measurements.

As part of the Photochemical Activity and Solar Ultraviolet Radiation (PAUR) project a measurement campaign took place in June 1996 in Athens–Tatoi and on a small Aegean island, Agios Efstratios. The campaign measured key chemical compounds and actinic fluxes as well as the surface UV irradiance and aerosol optical depth and ozone profiles.

In this paper the surface irradiance measurements are compared with a detailed radiative transfer model. The effect of aerosols are investigated by comparing simulated spectra with aerosol free model spectra.

The paper is organized as follows: first, the spectroradiometers used to measure the UV irradiance are described. A brief description of the radiative transfer model follows together with a discussion of the model input parameters. Next, the model simulations are compared with the measurements and subsequently used to investigate the effects of aerosols on surface UV irradiance. Finally, the results are summarized.

[1]Norwegian Institute for Air Research, Tromsø.

[2]Also at Geophysical Institute, University of Oslo.

[3]Physics Department, Laboratory of Atmospheric Physics, Aristotle University of Thessaloniki, Thessaloniki, Greece.

[4]Institute of Medical Physics, University of Innsbruck, Innsbruck, Austria.

Paper number 98JD02350.
0148-0227/98/98JD-02350$09.00

2. Spectroradiometers

Two double monochromator spectroradiometers were used, one Bentham DM 150 and one Brewer MK III. Both instruments have previously been described by *Gardiner and Kirsch* [1995] and *Bais* [1997]. The Bentham was located at the Tatoi airfield (38.112°N, 23.781°E, 255 m) outside Athens between June 7 and June 23, 1996. The Brewer was placed on Agios Efstratios (39.57°N, 24.97°E, 49 m) between June 2 and June 19. It was moved to Athens and operated next to the Bentham between June 21 and June 23 for intercomparison. During most of the period the sky was cloud free. Both instruments collected absolutely calibrated direct and global (direct plus diffuse) irradiance spectra every half hour.

2.1. Bentham DM 150 Spectroradiometer

The Bentham DM 150 instrument is a double monochromator with holographic gratings (2400 lines/mm). The bandwidth (full width at half maximum, or FWHM) is 0.72 nm, and each scan covers the wavelength range 290 to 500 nm with steps of 0.5 nm. A complete scan takes about 2 min. The spectroradiometer is calibrated against a 1000 W halogen lamp, traceable to Physikalisch-Technische Bundesanstalt, Germany. The instrument was checked for stability by calibration measurements before and after the campaign. During the campaign, stability was monitored by continuous comparison of the spectral data with data from a broadband meter. The overall uncertainty of the calibration is estimated to be ±5%.

The entrance optics consist of a flat Teflon diffuser. The deviation of the angular response of the diffuser from ideal cosine response was determined in the laboratory. A correction algorithm was used to correct the measured global irradiance for the imperfect cosine response of the diffuser. The algorithm takes into account the measured direct to global ratio and assumes an isotropic distribution of diffuse sky radiance. This assumption is less justified for longer wavelengths [*Gröbner et al.*, 1996]. *Blumthaler et al.* [1996] found spatial variations in the sky radiance by up to a factor of 10 in the UVA, which decreased to a factor of 2 in the UVB. The uncertainty of the cosine correction procedure is thus higher at longer wavelengths. However, for the conditions during the campaign the error in the cosine correction due to the isotropy assumption is estimated to be smaller than 0.5% [*Bais et al.*, 1998]. The magnitude of the cosine correction for the conditions during the campaign is of the order of 15%. The overall error due to the cosine correction procedure is estimated to be 2–4%.

Besides global irradiance the Bentham instrument also measures direct irradiance by changing the input optics at the end of a 2 m fiber from the diffuser to a small telescope with a field of view of about 1.5°. The measurements of direct Sun irradiance allows determination of total column ozone and of aerosol optical depth in the wavelength range 290 to 500 nm [*Huber et al.*, 1995]. The spectral dependence of aerosol optical depth, τ_{aerosol}, was fitted to the Ångström formula and characterized by the two parameters α and β:

$$\tau_{\text{aerosol}} = \beta\lambda^{-\alpha} \tag{1}$$

where the wavelength λ is in microns. In parallel to the Bentham spectroradiometer a Sun photometer (Noll Company, Germany) and an actinometer were used for control of the direct irradiance measurements. Only small statistical differences, less than ±5%, were observed throughout the campaign. Therefore the absolute uncertainty of the spectral aerosol optical depth measurements is estimated to be less than ±0.05 in the UV range.

2.2. Brewer MK III Spectroradiometer

The Brewer spectroradiometer is a double monochromator consisting of two identical spectroradiometers equipped with holographic diffraction gratings (3600 lines/mm) operating in the first order. Between the two spectroradiometers there are six band-selecting slits, which are opened sequentially to perform total ozone measurements, following the well-known methodology described by *Brewer* [1973]. For the spectral UV measurements, only one of the six slits is used. The operational spectral range of the instrument is 287.5–366.0 nm, and its spectral resolution is 0.55 nm (FWHM). The sampling interval is 0.5 nm, and a whole scan is completed in 8 min. The wavelength calibration is maintained by scanning the emission lines of an internal mercury lamp, and the absolute calibration is done by scanning a 1000 W National Institute of Standards and Technology traceable quartz-halogen tungsten standard lamp of spectral irradiance. A set of five 50 W lamps is used to track the stability of the instrument in the field.

The entrance optics of the instrument consist of a flat Teflon diffuser, used for measurements of the global solar irradiance, and a rotating prism that allows the measurement of the direct component. Because of imperfections in the design of the diffuser the global measurements are corrected for deviations from the ideal angular response. This is done by assuming isotropic distribution of sky radiance and taking into account the percentage of global to direct irradiance, both of which are measured by the Brewer. The magnitude of the correction for the conditions during the campaign ranged between 3% and 5%. The aerosol optical depth as a function of wavelength was determined from the direct measurements [*Marenco et al.*, 1997]. It was fitted to the Ångström formula in terms of Ångström α and β coefficients.

3. Radiative Transfer Model

The radiative transfer model used is similar to the one described by *Mayer et al.* [1997]. The radiative transfer equation is solved by the discrete ordinate algorithm

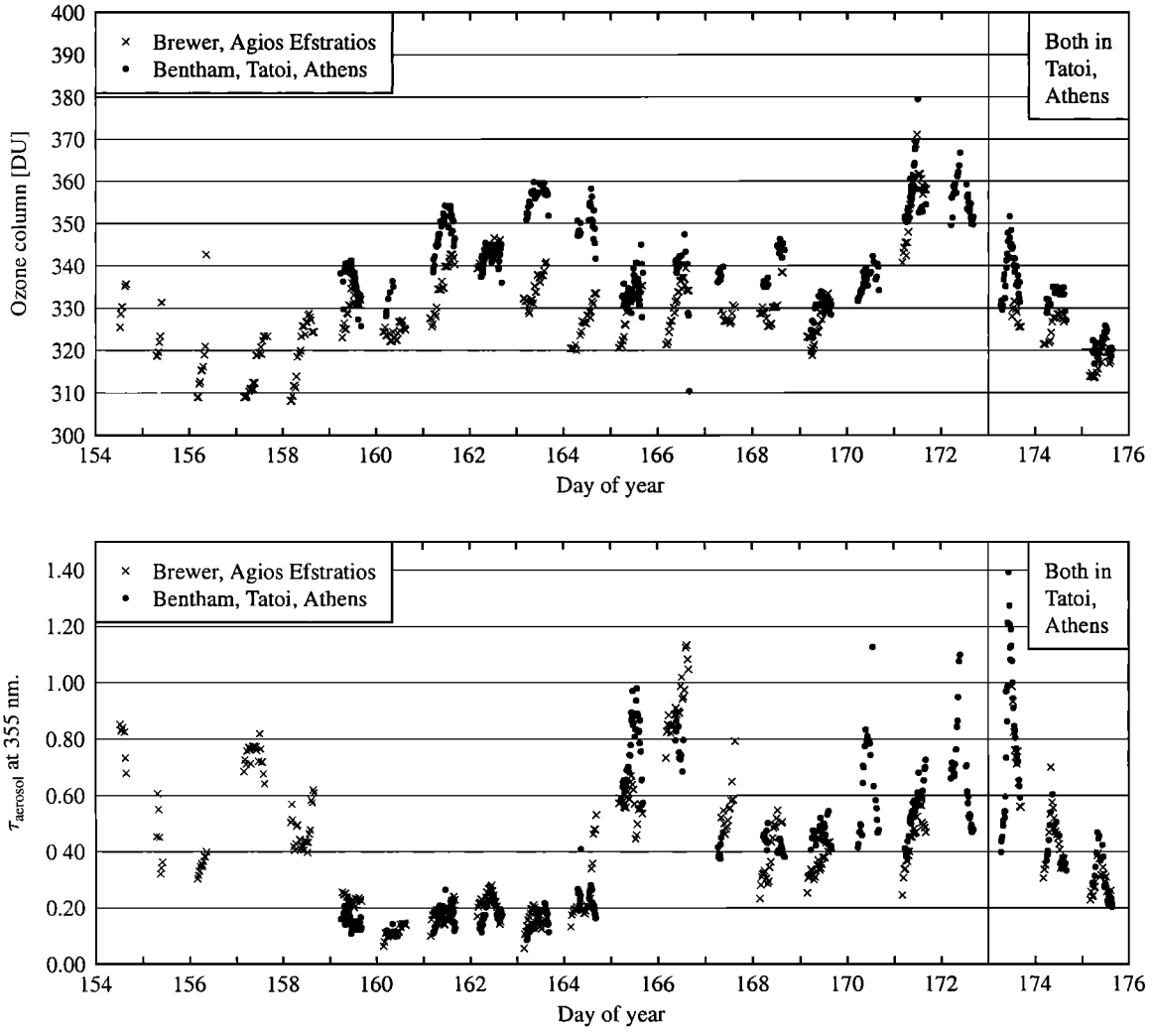

Figure 1. (top) Ozone column as measured by the Brewer and Bentham instruments. (bottom) Measured column aerosol optical depth at 355 nm. Between days 154 and 171 the Brewer instrument was located on the island of Agios Efstratios. From day 173 to 176 it was colocated with the Bentham instrument in Tatoi, Athens.

developed by *Stamnes et al.* [1988]. This algorithm has been modified to account for the spherical shape of the atmosphere using the pseudo–spherical approximation [*Dahlback and Stamnes*, 1991]. The pseudo–spherical radiative transfer equation solver was run in six–stream mode.

To simulate a measured global irradiance spectrum, the transmittance is calculated at 0.5 nm resolution, interpolated to higher, 0.05 nm, resolution using cubic splines, and multiplied with a high–resolution extraterrestrial spectrum corrected for the Earth–Sun distance. This high–resolution spectrum is convolved with the spectroradiometer slit function and interpolated to the center wavelengths of the measured spectrum [*Mayer et al.*, 1997].

Input to the radiative transfer model are the ozone profile; aerosol optical depth, single–scattering albedo, and phase function profiles; extraterrestrial spectrum; surface albedo; and time and location of the measurement. Changes in the solar zenith angle during a single scan are accounted for. Temperature dependent ozone cross sections are taken from *Bass and Paur* [1985]. The Rayleigh scattering cross section is calculated according to the formula of *Nicolet* [1984].

4. Measured Model Input Parameters

The ozone column and aerosol optical depth column were deduced from the direct Sun spectra recorded by the spectroradiometers. Ozone and aerosol optical depth profiles were measured by ozone sondes and aerosol lidar, respectively.

4.1. Ozone and Aerosol Optical Depth Columns

The ozone column and aerosol optical depth for the whole campaign period is shown in Figure 1. Considering that the two observation sites are approximately 200 km apart and that one is located on a pristine island

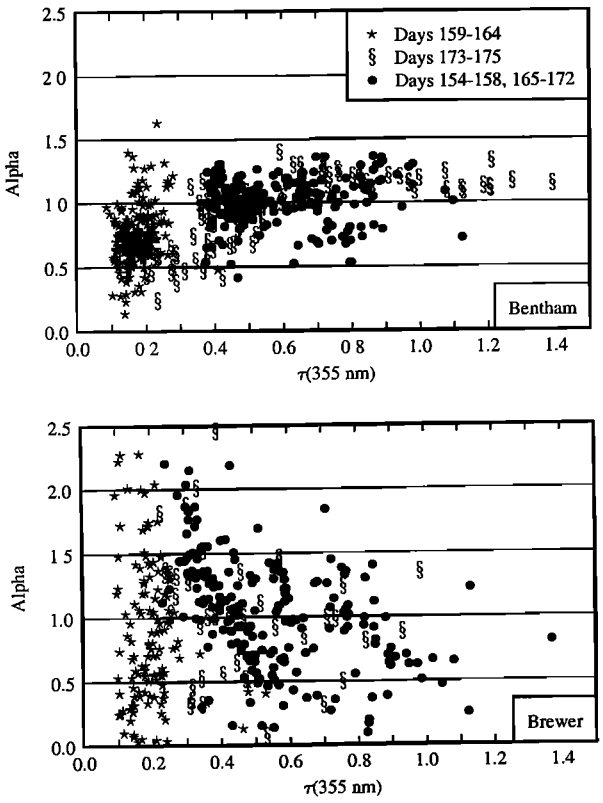

Figure 2. Ångström coefficient α versus the aerosol optical depth at 355 nm, $\tau(355\ \text{nm})$, as measured by the (top) Brewer and (bottom) Bentham instrument. For days 173–175, both instruments were colocated in Tatoi, Athens.

and the other close to a major city, the aerosol optical depths are strikingly similar for the two sites. During the campaign, northeasterly winds were dominating. Hence both observation sites were exposed to fairly similar air masses. Thus, for the aerosol conditions during the campaign period, large–scale circulation was more important than local disturbances. Except for days 163 and 164, when the ozone column was about 20 Dobson units (DU) higher over Athens, the ozone columns are similar for the two sites. The differences for days 163 and 164 are explained by an "edge" in the ozone distribution as seen in the TIROS operational vertical sounder (TOVS) instrument data.

The two spectroradiometers were operated next to each other in Athens between June 21 and 23. The agreement between the aerosol optical depth measured by the two instruments is very good, see Figure 1 (bottom). The differences between the ozone columns are within the experimental uncertainty of approximately ±2.0%.

While it is beyond the scope of the present work to give a detailed study of the origin and composition of aerosols during the PAUR campaign, the measured Ångström α coefficient versus $\tau(355\ \text{nm})$ is shown in Figure 2. For days 159–164 the aerosol content was relatively low, $\tau(355\ \text{nm}) < 0.3$ (Figure 1). For these days the α coefficients vary between 0.1 and 1.6 (Bentham). Large values of α may be interpreted as the presence of small aerosol particles, while small values of α are due to large aerosol particles. Hence the span of α coefficients for days 159–164 might indicate a variety of aerosol types and corresponding size distributions. For the more turbid days, 154–158 and 165–175, the α coefficients measured by the Bentham are clustered around unity, thus indicating that for aerosol optical depths $\tau(355\ \text{nm}) > 0.3$ the aerosols are more uniform and larger in size. The α coefficients reported from the Brewer generally show the same clustering of the α–τ relationship as the Bentham; however, the data are more spread out. This behavior may be caused by the smaller wavelength range of the Brewer, since a smaller wavelength range gives larger uncertainties in the determination of the α coefficients. While $\tau(355\ \text{nm})$ decreases for increasing solar zenith angles (compare Figure 1), the α coefficient exhibits no clear solar zenith angle dependence.

4.2. Ozone and Aerosol Optical Depth Profiles

Information about the vertical distribution of ozone was obtained from ozone sondes launched from Thessaloniki on June 4, 6, 8, 10, 11, and 13, 1996 (see Figure 3). The vertical distribution of the aerosol optical depth was measured by an aerosol lidar on the island of Agios Efstratios between June 5 and 14 [*Marenco et al.*, 1997]. The aerosol optical profile was measured at 355 and 532 nm. Since interest here is in the UV, only the shortest wavelength is used. Both lidar wavelengths may be used to calculate altitude dependent Ångström coefficients. However, because of considerable noise in the lidar measurements the Ångström coefficients estimated from the spectroradiometer measurements were used. The aerosol optical depth was measured in the altitude range 600–6000 m depending on conditions. The aerosol loading in the stratosphere was negligible during the PAUR campaign [*Marenco et al.*, 1997].

Both the aerosol profile and the ozone profile were smoothed with a triangular function with a FWHM of 400 m and interpolated to 400 m resolution using cubic splines. The aerosol optical depth profile was assumed constant below 600 m. Above 6000 m the aerosol optical depth was set to zero. Daily averaged aerosol optical depth profiles are shown in Figure 4. For the ozone profile a constant mixing ratio was assumed above the balloon burst altitude.

For a specific radiative transfer simulation of a measurement the aerosol optical depth and ozone profiles closest in time were chosen. The aerosol optical depth and ozone profiles were scaled to the aerosol optical depth and ozone column measured by the spectroradiometers. Both the Brewer and the Bentham ozone retrieval algorithms utilize the ozone cross sections from *Bass and Paur* [1985]. The same ozone cross sections were used for the model simulations.

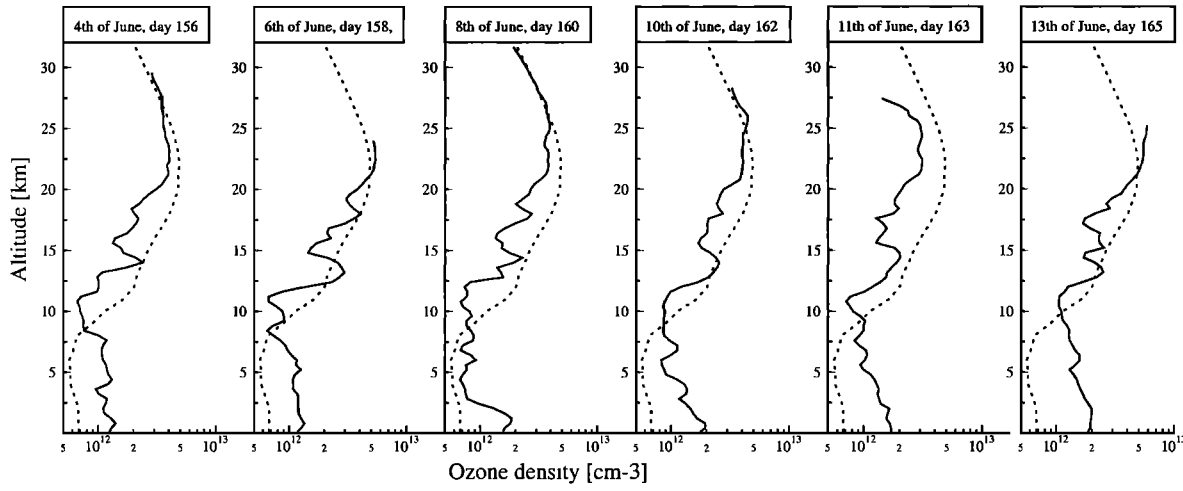

Figure 3. Ozone concentration (solid lines) measured by ozone sondes launched from Thessaloniki, Greece. The ozone profiles have been smoothed with a triangular function with a full width at half maximum (FWHM) of 400 m and interpolated to 400 m resolution using cubic splines. Included for reference is the U.S. standard profile (dotted lines, *Anderson et al.* [1986]).

The extraterrestrial spectrum was adopted from several sources. Between 280 and 407.8 nm the Atlas 3 spectrum shifted to air wavelengths (M. E. VanHoosier, personal communication, 1996) was used. Atlas 2 [*Woods et al.*, 1996] was used between 407.8 and 419.9 nm. Above 419.9 nm the solar spectrum in the Modtran 3.5 radiation model was used [*Anderson et al.*, 1993].

5. Assumed Model Input Parameters

No information was available about the effective surface albedo "seen" by the spectroradiometers. The Brewer on the island of Agios Efstratios was located on a dry sandy hilltop close to the sea. The Bentham was in an area surrounded by forest. Albedos in the UV for snow free surfaces are typically small [*Blumthaler and Ambach*, 1988]. Surface reflectivities at 380 nm estimated from total ozone mapping spectrometer data for this region are in the 3–5% range [*Herman and Celarier*, 1997]. A surface albedo of 0.03 was used in the present study. Small variations in the surface albedo will only marginally affect the model results [*Schwander et al.*, 1997; *Weihs and Webb*, 1997].

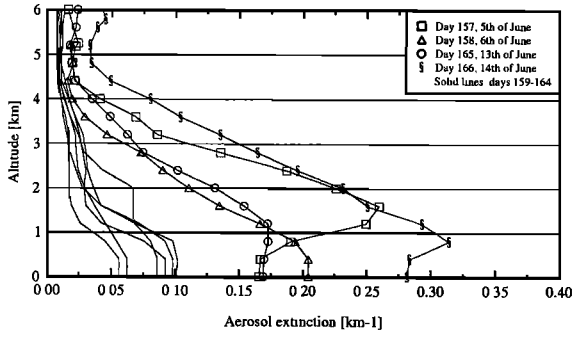

Figure 4. Smoothed and daily averaged aerosol optical depth profiles as measured by the lidar on Agios Efstratios at 355 nm. The aerosol profiles have been smoothed with a triangular function with a FWHM of 400 m and interpolated to 400 m resolution using cubic splines.

The composition of the aerosols during the PAUR campaign is not known. Hence direct information on the aerosol single–scattering albedo and phase function is not available. Initial comparisons between the radiative transfer model and the measured irradiances were performed with a fixed value for the aerosol single–scattering albedo, $\omega = 0.87$, and using a Heyney–Greenstein phase function with a fixed asymmetry factor, $g = 0.7$. These values were chosen because they gave the overall best agreement between model and measurement for the period both spectroradiometers were colocated in Tatoi, Athens (see values in parentheses in Table 1).

However, the use of the same aerosol single–scattering albedo and asymmetry factor for all days resulted in large day–to–day variations in the model/measurement ratio; see Figure 5 (left). Hence it was decided to vary the aerosol single–scattering albedo from day to day but to keep it constant for each individual day. The value of the aerosol single–scattering albedo for a specific day was taken to be the value that gave the best agreement between model and measurement at noon. The adopted values are shown in Figure 6. The mean (standard deviation) of the single–scattering albedo for the campaign period was 0.92 (5%) for the Brewer data and 0.91 (5.6%) for the Bentham data. The aerosol asymmetry factor was fixed at 0.70. Varying the asymmetry factor between 0.5 and 1.0 for a fixed aerosol single–scattering albedo caused changes in the

Table 1. Mean and Standard Deviation for the UVB and UVA Model/Measurement Ratios

Instrument	Athens		Whole Period	
	Mean	Standard Deviation	Mean	Standard Deviation
		UVB (280 -315 nm)		
Brewer Mk III	1.034 (1.050)	0.024 (0.031)	1.035 (0.986)	0.043 (0.062)
Bentham DM150	0.950 (0.964)	0.034 (0.041)	0.973 (0.931)	0.050 (0.063)
		UVA (315 -365 nm)		
Brewer Mk III	1.019 (1.034)	0.019 (0.031)	1.023 (0.977)	0.024 (0.056)
Bentham DM150	0.952 (0.965)	0.032 (0.039)	0.976 (0.936)	0.040 (0.059)

UVB is defined as the integrated irradiance between 280–315 nm, while UVA is defined as the integrated irradiance between 315–365 nm. The upper limit on UVA is due to the wavelength range scanned by the Brewer instrument. For the Athens period a total of 49 Brewer (84 Bentham) measurements are compared with model simulations. For the whole period, 390 and 454 measurements are included from the Brewer and Bentham instruments, respectively. The aerosol single–scattering albedo was varied as shown in Figure 6. Parentheses show results using a fixed aerosol single–scattering albedo ($\omega = 0.87$). See text for explanation.

model/measurement ratios of the order of ±4%. Both the aerosol single–scattering albedo and the asymmetry factor were assumed to be constant with altitude.

Since no independent information is available on the absorption and scattering characteristics of the aerosols during the campaign, it is difficult to say with confidence that the changes in the aerosol single–scattering albedo are realistic. However, the variations seen may be encompassed by standard aerosol models. Also, information from the diffuse radiation field, which is part of the global radiation field used to estimate the aerosol single–scattering albedo, has been used to estimate the aerosol refractive index [*King*, 1979; *King and Herman*, 1979]. The aerosol single–scattering albedo undoubtedly has a diurnal variation. However, it is beyond the scope of this work to derive and study the diurnal changes in the aerosol single–scattering albedo and asymmetry factor.

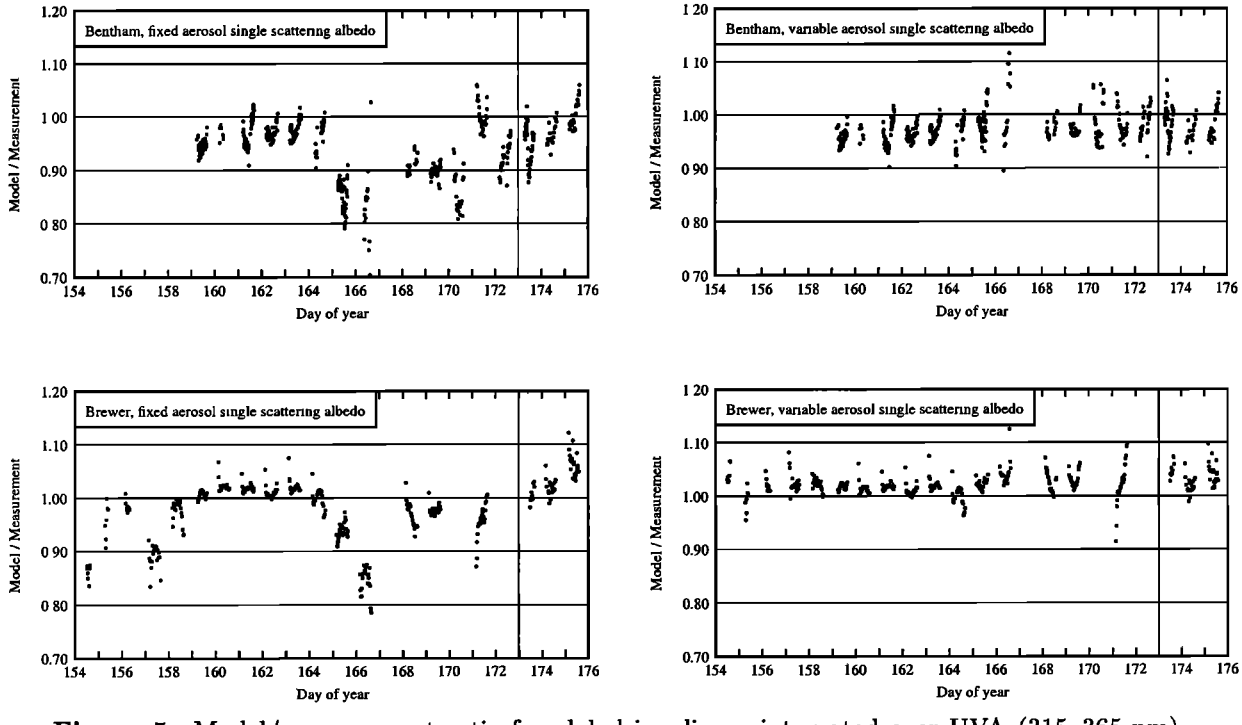

Figure 5. Model/measurement ratio for global irradiance integrated over UVA (315–365 nm) as a function of time. (left) Fixed aerosol single–scattering albedo, $\omega = 0.87$, used for the model simulations. (right) The aerosol single–scattering albedo was varied from day to day as shown in Figure 6. After day 171 (vertical line) both instruments were colocated in Tatoi, Athens. A total of 390 (454) Brewer (Bentham) measurements are compared with model simulations.

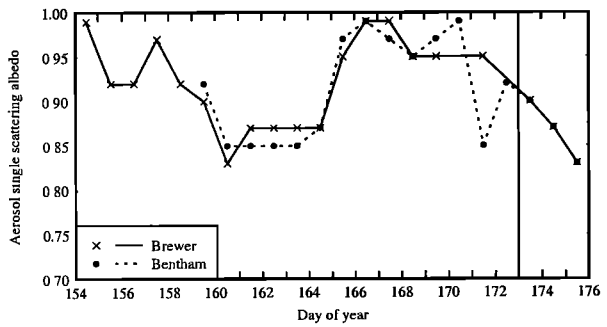

Figure 6. Assumed daily aerosol single–scattering albedo used for the model simulations of the measured irradiances.

6. Model/Measurement Comparison

For the PAUR campaign a total of 390 (454) global irradiance spectra measured by the Brewer (Bentham) instrument were simulated by the model. One typical example of the ratios between simulated and measured spectra is shown in Figure 7 (top). Both the model/Brewer and model/Bentham ratios are fairly constant with wavelength. The fluctuations may be attributed to remaining differences between the actual slit function of the measurement and the one used by the model, and Raman scattering (Ring effect), which is not accounted for by the model. Above 420 nm the fluctuations increase in magnitude. This increase is believed to be caused by the extraterrestrial spectrum used by the model in this region. The slight differences in the model/measurement ratios below 320 nm may be attributed to uncertainties in the ozone column.

The model/Brewer ratio is 4–5% larger than the model/Bentham ratio (Figure 7). This difference is also apparent for integrated UVB and UVA (Table 1). It may be explained by differences in the absolute calibration of the two instruments and by uncertainties due to the cosine correction procedures.

The differences between the model simulations and measurements are comparable in magnitude to the results reported by *Mayer et al.* [1997]. The *Mayer et al.* [1997] measurement/model ratio increased from ≈0.9 to ≈1.0 between 300 and 365 nm, whereas the present results are relatively flat. Recent investigations have shown that the wavelength dependent results of *Mayer et al.* [1997] were partly caused by small nonlinearities of the system. Correcting for the nonlinearity gives better agreement between the measurements and the model simulations (B. Mayer, personal communication, 1998).

The UVA model/measurement ratios as a function of time are shown in Figure 5. The mean and standard deviation of the UVB and UVA model measurements ratios for the whole period are given in Table 1. The daily variations have at least two possible sources: first, the uncertainties in the cosine error correction algorithms, and second, the assumption made about the aerosol optical properties. An excessively high aerosol single–scattering albedo in the model will give too much diffuse radiation. Since the ratio diffuse/global irradiance increases with increasing solar zenith angle, the model/measurement ratio will also increase with increasing solar zenith angle if the aerosol single–scattering albedo in the model is too high. Hence since the aerosol single–scattering albedo was constant for each day, a daily variation in the model/measurement ratio may occur. With no information available about the aerosol single–scattering albedo and phase function from other independent simultaneous measurements, no check could be made about which values were representative for the actual atmospheric situation.

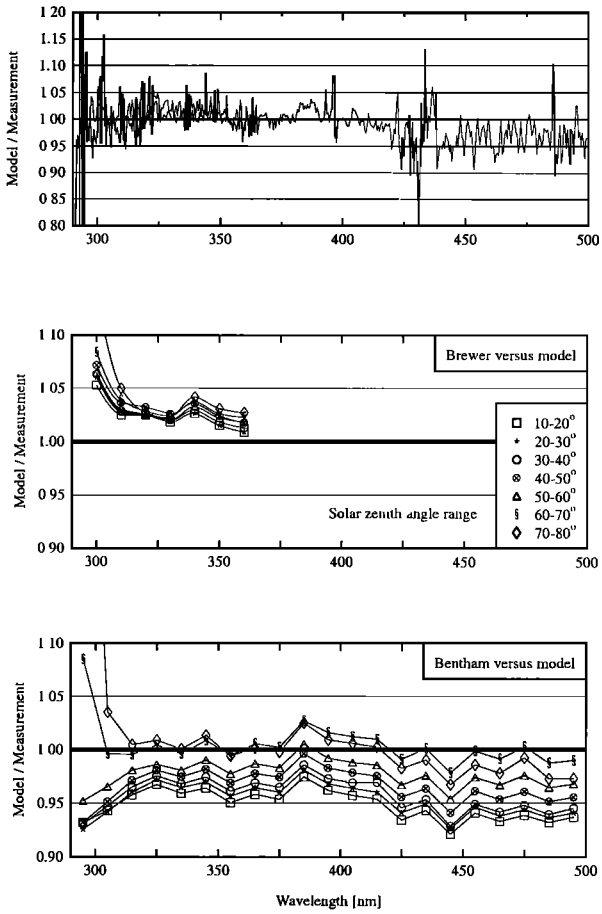

Figure 7. (top) Ratio of simulated and measured global irradiances for June 23, 1996. The Brewer (Bentham) measurement covers the wavelength range 287.5–366.0 (290.0–500.0) nm and was made at 1200 (1152) UTC. The instruments were located next to each other in Tatoi, Athens. (middle, bottom) Model/measurement ratios as a function of solar zenith angle and wavelength where data were averaged over intervals of 10 nm wavelength and 10° solar zenith angle. A total of (middle) 390 total spectra recorded by the Brewer instrument on Agios Efstratios and in Athens and (bottom) 494 total spectra recorded by the Bentham in Athens are compared with model simulations.

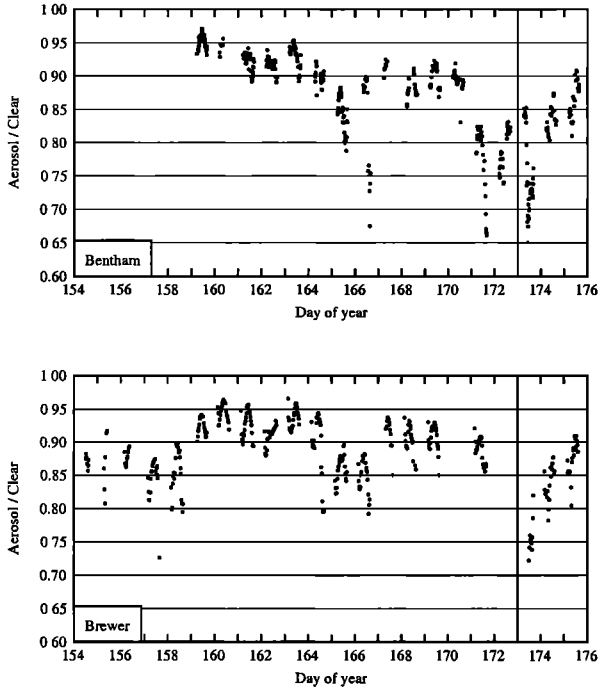

Figure 8. Ratio between UVB (280–315 nm) dose rates from simulated spectra including aerosols and spectra without aerosols.

7. Effect of Aerosols on Surface UV Irradiance

The model–simulated spectra may be used to investigate the effect of aerosols on the surface UV irradiance. The simulated spectra were recalculated without aerosols. The ratio between simulated spectra with and without aerosols is shown in Figure 8. The presence of aerosols is seen to reduce the UVB irradiance by a fraction ranging between 5% and 35%. For the UVA the effect is similar but approximately 5% smaller. The reduction is of course anticorrelated with the aerosol optical depth (Figure 1).

Figure 9 shows measured UVB irradiances as a function of the ozone column. The UVB irradiances have been grouped into 10° solar zenith angle intervals. Idealized model calculations are also shown for each 10° solar zenith angle (solid lines). The variations in the measured values are nicely explained by the idealized model calculations for solar zenith angles larger than 30°. For the measured data in the 10°–20° and 20°–30° intervals there is a large spread in comparison with the model calculations. This is due to differences between the aerosol optical depth and single–scattering albedo used for the model calculations and the actual aerosol properties. In addition, there is uncertainty in the measured UVB irradiances and ozone columns. Similar arguments explain the spread in the 20°–30° interval data in comparison with the idealized model calculations.

The same measured UVB irradiances as a function of the aerosol optical depth at 355 nm are shown in

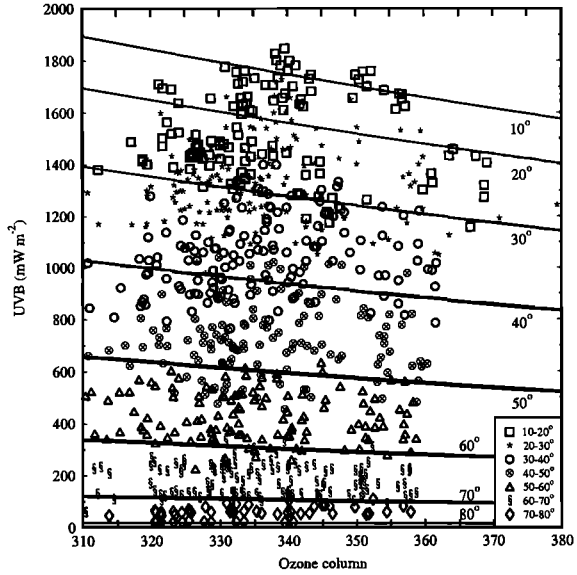

Figure 9. Measured Brewer and Bentham UVB dose rates versus ozone column for various solar zenith angles. The solid lines are model calculations for fixed solar zenith angles. The ozone profile was taken from the U.S. Standard Atmosphere [*Anderson et al.*, 1986]. It was scaled to the various ozone values. For the aerosols the background aerosol profile of *Shettle* [1989] was used. The aerosol single–scattering albedo was set to 0.87, the asymmetry factor was set to 0.7, and the surface albedo was 0.03. The aerosol optical depth was scaled by using Ångström coefficients $\alpha = 1.0$ and $\beta = 0.15$ (i.e., $\tau(355\text{ nm})=0.42$).

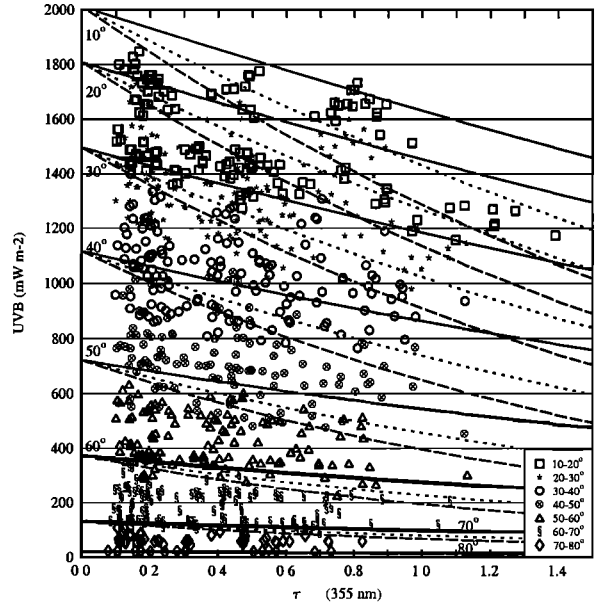

Figure 10. Measured Brewer and Bentham UVB dose rates versus aerosol optical depth at 355 nm for various solar zenith angle intervals. The various lines are model calculations for fixed solar zenith angles, an ozone column of 340 Dobson Units (DU) and Ångström coefficient $\alpha = 1.0$. The aerosol single–scattering albedo was 0.95 (solid line), 0.87 (dotted line), and 0.80 (dashed line).

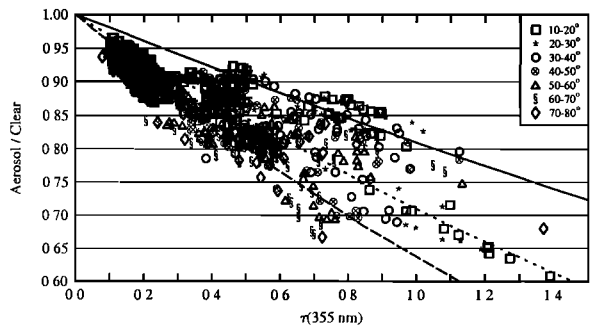

Figure 11. Ratio between simulated Brewer and Bentham UVB dose rates with and without aerosols as a function of the aerosol optical depth at 355 nm. Ratios of model results with an aerosol single–scattering albedo of 0.95 (solid line), 0.87 (dotted line), and 0.80 (dashed line) versus aerosol free model results are shown for a solar zenith angle of 10° and an ozone column of 340 DU.

Figure 10 together with idealized model calculations. The idealized model calculations explain most of the behavior of the measurements. As for Figure 9, remaining differences are due to different values for the measured ozone column and α coefficients compared with the model calculations. Also for Figure 9, there is some experimental uncertainty involved: in the determination of the ozone column and the Ångström α and β coefficients and in the UVB irradiance measurements.

It is evident from Figures 9 and 10 that variations in the solar zenith angle have the largest effect on the UV irradiance. Comparing Figures 9 and 10, we also find that for the conditions during the PAUR campaign the changes in the aerosol loading caused larger variations in the surface UV irradiance than variations in the ozone column. This finding is also illustrated by the model calculations presented in Figures 9 and 10.

Figure 11 shows the ratio of simulated UVB dose rates with and without aerosols as a function of the aerosol optical depth at 355 nm. Ratios based on idealized model calculations are also shown for various values of the aerosol single–scattering albedo. Independent of the solar zenith angle the UVB irradiance decreases with increasing aerosol loading. The magnitude of the decrease strongly depends on the value of the aerosol single–scattering albedo. A smaller ω absorbs more radiation and hence reduces the UV irradiance more for similar τ(355 nm).

8. Conclusions

UV direct and global irradiance measurements have been made under noncloudy conditions at two sites in Greece during the PAUR campaign, June 1996. The ozone column and aerosol optical depth were derived from the direct irradiance measurements. The measured global irradiances were compared with model simulations using measured ozone and aerosol optical depth profiles, and the impact of aerosols on the UV irradiance was investigated. The following results were found:

1. Large day–to–day and diurnal variations were observed in the aerosol optical depths. The optical properties of the aerosols present during the period between days 159 and 164 are distinctly different from those on the other days, as is evident from the total aerosol optical depth (Figure 1), the Ångström α coefficient (Figure 2), the aerosol optical depth profile (Figure 4), and the aerosol single–scattering albedo (Figure 6).

2. Overall the agreement between model simulations and measurements is good. The absolute differences between model and measurements and the standard deviations in Table 1 may be explained by the systematic errors of both the model and the measurements, by the uncertainties in the absolute calibration of the spectroradiometers, and by assumptions made about the aerosol optical properties.

3. The aerosol single–scattering albedo has a large effect on the model/measurement ratios.

4. In comparison with an aerosol free sky the aerosol loading during the PAUR campaign reduced the UVB irradiance by 5–35%.

5. For the campaign period, changes in the aerosol loading are found to cause larger variations in the UV irradiance than changes in the ozone column.

6. Information on aerosol composition, and in particular the aerosol single–scattering albedo and phase function, is of great importance for the impact studies of aerosol. While such information is not easily measured on a campaign basis, it is urgently needed.

The libRadtran radiative transfer model used for the simulations is available from our anonymous ftp site (ftp://ftp.geofysikk.uio.no/pub/outgoing/arveky).

Acknowledgments. We would like to thank F. Marenco and V. Santacesaria for providing us with the aerosol lidar data. This work was done within the framework of the PAUR project funded by the European Commission (contract ENV4-CT95-0048). A.K. acknowledges support from the European–funded UVRAPPF (contract ENV4-CT95-0165) and SUVDAMA (contract ENV4-CT95-0177) projects, and the Norwegian Research Council, to develop the radiative transfer model.

References

Anderson, G., S. Clough, F. Kneizys, J. Chetwynd, and E. Shettle, AFGL atmospheric constituent profiles (0-120 km), *Tech. Rep. AFGL-TR-86-0110*, Air Force Geophys. Lab., Hanscom Air Force Base, Bedford, Mass., 1986.

Anderson, G. P., J. H. Chetwynd, J.-M. Theriault, P. K. Acharya, A. Berk, D. C. Robertson, F. X. Kneizys, M. L. Hoke, L. W. Abreu, and E. P. Shettle, MODTRAN2: Suitability for remote sensing, in *Atmospheric Propagation and Remote Sensing, SPIE Conf. Ser.* vol. 1968, edited by A. Kohnle and W. B. Miller, pp. 514–525, Soc. of Photo–Instrum. Eng., Bellingham, Wash., 1993.

Bais, A. F., Absolute spectral measurements of direct solar ultraviolet irradiance with a Brewer spectrophotometer, *Appl. Opt.*, *36*, 5199–5204, 1997.

Bais, A. F., S. Kazadzis, D. Balis, C. S. Zerefos, and M. Blumthaler, Correcting global solar ultraviolet spectra recorded by a Brewer spectroradiometer for its angular response error, *Appl. Opt., in press*, 1998.

Bass, A. M., and R. J. Paur, The ultraviolet cross-section of ozone, I, The measurements, in *Atmospheric Ozone: Proceedings of the Quadrennial Ozone Symposium*, edited by C. S. Zerefos and A. Ghazi, pp. 606–601, D. Reidel, Norwell, Mass., 1985.

Blumthaler, M., and W. Ambach, Solar UVB-albedo of various surfaces, *Photochem. Photobiol.*, *48*, 85–88, 1988.

Blumthaler, M., J. Gröbner, M. Huber, and W. Ambach, Measuring spectral and spatial variations of UVA and UVB sky radiance, *Geophys. Res. Lett.*, *23*, 547–550, 1996.

Brewer, A. W., A replacement for the Dobson spectrophotometer, *Pure Appl. Geophys.*, *106–108*, 919–927, 1973.

Dahlback, A., and K. Stamnes, A new spherical model for computing the radiation field available for photolysis and heating at twilight, *Planet. Space Sci.*, *39*, 671–683, 1991.

Gardiner, B. G., and P. J. Kirsch, Setting standards for European ultraviolet spectroradiometers, *Air Pollut. Res. Rep. 53*, Comm. of Eur. Commun., Brussels, Belgium, 1995.

Gröbner, J., M. Blumthaler, and W. Ambach, Experimental investigation of spectral global irradiance measurement errors due to a non ideal cosine response, *Geophys. Res. Lett.*, *23*, 2493–2496, 1996.

Herman, J. R., and E. A. Celarier, Earth surface reflectivity climatology at 340–380 nm from TOMS data, *J. Geophys. Res.*, *102*, 28,003–28,011, 1997.

Huber, M., M. Blumthaler, W. Ambach, and J. Staehelin, Total atmospheric ozone determined from spectral measurements of direct solar UV irradiance, *Geophys. Res. Lett.*, *22*, 53–56, 1995.

King, M. D., Determination of the ground albedo and the index of absorption of atmospheric particulates by remote sensing, II, Application, *J. Atmos. Sci.*, *36*, 1072–1083, 1979.

King, M. D., and B. M. Herman, Determination of the ground albedo and the index of absorption of atmospheric particulates by remote sensing, I, Theory, *J. Atmos. Sci.*, *36*, 163–173, 1979.

Liu, S. C., S. A. McKeen, and S. Madronich, Effect of anthropogenic aerosols on biologically active ultraviolet radiation, *Geophys. Res. Lett.*, *18*, 2265–2268, 1991.

Marenco, F., V. Santacesaria, A. F. Bais, D. Balis, A. di Sarra, A. Papayannis, and C. Zerefos, Optical properties of tropospheric aerosols determined by lidar and spectrophotometric measurements (Photochemical Activity and Solar Ultraviolet Radiation campaign), *Appl. Opt.*, *36*, 6875–6886, 1997.

Mayer, B., G. Seckmeyer, and A. Kylling, Systematic long-term comparison of spectral UV measurements and UVSPEC modeling results, *J. Geophys. Res.*, *102*, 8755–8767, 1997.

Nicolet, M., On the molecular scattering in the terrestrial atmosphere: An empirical formula for its calculation in the homosphere, *Planet. Space Sci.*, *32*, 1467–1468, 1984.

Schwander, H., P. Koepke, and A. Ruggaber, Uncertainties in modeled UV irradiances due to limited accuracy and availability of input data, *J. Geophys. Res.*, *102*, 9419–9429, 1997.

Shettle, E. P., Models of aerosols, clouds and precipitation for atmospheric propagation studies, paper presented at Conference on Atmospheric Propagation in the UV, Visible, IR and MM-Region and Related System Aspects, NATO Adv. Group for Aerosp. Res. and Dev., Copenhagen, 1989.

Stamnes, K., S.-C. Tsay, W. Wiscombe, and K. Jayaweera, Numerically stable algorithm for discrete-ordinate-method radiative transfer in multiple scattering and emitting layered media, *Appl. Opt.*, *27*, 2502–2509, 1988.

Weihs, P., and A. R. Webb, Accuracy of spectral UV model calculations, 1, Consideration of uncertainties in input parameters, *J. Geophys. Res.*, *102*, 1541–1550, 1997.

Woods, T. N., et al., Validation of the UARS solar ultraviolet irradiances: Comparison with the Atlas 1 and 2 measurements, *J. Geophys. Res.*, *101*, 9541–9569, 1996.

A. Kylling, NILU-Tromsø, N-9005 Tromsø, Norway. (e-mail: arve.kylling@nilu.no)

A. F. Bais, C. S. Zerefos, and E. Kosmidis, Laboratory of Atmospheric Physics, Physics Department, Aristotle University of Thessaloniki, 540 06 Thessaloniki, Greece. (e-mail: abais@ccf.auth.gr; zerefos@olymp.ccf.auth.gr; ekosmidis@ccf.auth.gr)

M. Blumthaler and J. Schreder, Institute of Medical Physics, Müllerstrasse 44, A-6020 Innsbruck, Austria. (e-mail: Mario.Blumthaler@uibk.ac.at)

(Received February 26, 1998; revised July 8, 1998; accepted July 13, 1998.)